X-ray Diffraction Technique with Imaging Plate for Detecting Surface Distribution of Residual Stress in Diaphysis of Bovine Femurs

Satoshi YAMADA[a], Shigeru TADANO[a,*], Mai ONUMA[b]

[a] Division of Human Mechanical Systems and Design, Faculty of Engineering, Hokkaido University, N13 W8, Kita-ku, Sapporo, Hokkaido 060-8628, Japan

[b] Division of Human Mechanical Systems and Design, Graduate School of Engineering, Hokkaido University, N13 W8, Kita-ku, Sapporo, Hokkaido 060-8628, Japan

*Corresponding Author:
Shigeru TADANO, PhD
Professor, Division of Human Mechanical Systems and Design, Faculty of Engineering, Hokkaido University, N13 W8, Kita-ku, Sapporo, Hokkaido 060-8628, JAPAN
Tel/Fax: +81(JAPAN)-11-706-6405
E-mail: tadano@eng.hokudai.ac.jp

Word count: 3842 words (Introduction through Acknowledgments)
Type of manuscript: Research paper
Keywords: Biomechanics, Bone, X-ray Diffraction, Imaging Plate, Residual Stress

Abstract

Stress measurements of bone are essential for evaluating the risk of bone fracture, the cure of bone diseases (e.g., osteoporosis), and the bone adaptation. Previously, a method using X-ray diffraction (XRD) was used to assess the presence of residual stress in the diaphysis of bovine and rabbit extremities. However, the previous method required a complicated experimental setup, long irradiation time, and limitations of the sample size. To profoundly enhance the understanding of distribution and biomechanical implications of bone residual stresses, it is necessary to develop an alternative method that features a simple setup without limitations on the sample size and shape. An imaging plate (IP) can obtain the two-dimensional distribution of hydroxyapatite crystal deformation and has the potential to resolve the previously mentioned issues. The aim of this study was to develop a measurement system using an XRD technique with an IP for obtaining the surface distribution of residual stress in the diaphysis of extremities. A mid-diaphysis specimen taken from an adult bovine femur was irradiated with characteristic Mo-Kα X-rays under no external forces and the diffracted X-rays were detected by an IP in the reflection side. The residual stress in the

bone axis was calculated from the XRD pattern. As a result, tensile residual stresses were detected at the diaphyseal surface, corresponding to the results of the previous method. The developed system reduced the irradiation time by two thirds and the limitations of the sample size were removed. (239 words)

1. Introduction

Stress measurements of bone are essential for evaluating the risk of bone fracture, the cure of bone diseases (e.g., osteoporosis), and the bone adaptation. Researches attempted to obtain in vivo measurements of bone strain under external loads by invasive procedures with strain gauges glued to the bone surface, as reviewed by Al Nazer et al. [1]. The surface stress/strain state is important in cortical bone of the extremities because it is subjected to external compression, bending, and/or torsion loads in vivo. X-rays have nondestructive and noninvasive properties, therefore X-ray diffraction (XRD) is a promising tool to obtain in vivo measurements of the stress/strain in cortical bone [2]. The deformation of hydroxyapatite (HAp) crystals in bone tissue and tooth was measured under external loads using XRD as reported in the literature, e.g. [3-16]. Fujisaki and Tadano presented the relationship between bone tissue strain and HAp crystal strain in bovine cortical bone under tensile loads in vitro [6] and, Almer and Stock investigated the strain and stress of the mineral phase in canine fibular diaphysis under compressive loads in vitro [3, 7]. Further, the stress/strain state in cortical bone samples under no external forces was measured from the deformed HAp

crystals and the presence of residual stress in the diaphysis of bovine and rabbit extremities was reported [17-22].

Residual stress is defined as the stress that remains in bone tissue without any external forces. The residual stress is one of the stress applied to bone tissue as well as static stresses due to body weight and dynamic stresses due to movement. Residual stress will be one of the important factors to understand the bone strength and bone adaptation. Generally, the residual stress is a significant factor for the strength of a material. In fact, blood vessel walls are subject to residual stresses, which may decrease high external stresses that are due to blood pressure [23]. On bone tissue, the surface region in the diaphysis of extremities is subjected to tensile residual stresses along the bone axis, which may decrease high external stresses in the surface due to in vivo compression and bending [19-22]. Further, the magnitude of residual stresses correlated with the osteon population density [20]. Osteons are generated in cortical bone during bone formation and reconstruction and are related to the mechanical environment in vivo [24-25]. It suggests that the residual stress is related to the bone formation and reconstruction, and the stress may be a circumstantial finding of the adapted state of the

bone. Further, from [22], young bovine femurs showed not to be subjected to residual stresses, whereas larger residual stresses were observed in mature femurs. This suggests that the residual stresses are generated during growth. However, the surface distribution and biomechanical implications of the residual stress are not fully understood.

In a previous study, the $\sin^2\psi$ method was proposed to measure residual stress at the surface of cortical bones [19]. In the method, the residual stress of bone tissue was estimated from the variation of the interplanar spacing of HAp crystals without a comparison against non-strained samples or information on the interplanar spacing in the stress direction. However, the method required a complicated experimental setup, long irradiation time, and limitations of the sample size in the longitudinal direction because rotating and tilting the sample is required to obtain the distribution of the HAp crystal deformation. Hence the method could not be directly applied to the measurements of residual stress distribution in situ and in vivo. To profoundly enhance the understanding of distribution and biomechanical implications of residual stress in bone tissue, it is necessary to develop an alternative method that features a simple setup without limitations on the sample size and shape.

An imaging plate (IP), which is a two-dimensional X-ray detector, can obtain the distribution of the diffracted X-rays from the HAp crystals with only one irradiation. The distribution of the HAp crystal deformation can then be calculated from the XRD pattern detected via the IP. Giri et al. reported on the site-specific residual strain around the foramen in bovine bones from the diffracted X-rays that penetrated the specimens and then were detected by the IP; however, the specimens were required to be sliced [18]. Almer and Stock conducted in vitro stress/strain measurements of canine fibular diaphyses using high-energy X-rays with a two-dimensional X-ray detector [3, 7]. In their studies, the diffracted X-rays transmitted through the diaphysis were detected and the stress/strain in the mineral phase was the weighted average of the X-ray pathway from the irradiated surface to the opposite surface of the diaphysis. However, these methods cannot obtain the surface distribution of residual stresses.

The aim of this study was to develop a measurement system using an XRD technique with the IP set in the reflection side (XRD-IP system) for obtaining the surface distribution of residual stress in the diaphysis of extremities without limitations of the sample size and long irradiation time.

2. Materials and methods

2.1 Specimen preparation

The mid-diaphysis part of a cortical bone in an adult bovine femur was used in this study. The diaphysis specimen was 60 mm long in the bone axis and cut using a slow speed diamond wheel saw (Model 650: South Bay Technology Inc., USA). An identical specimen was used to compare the results for both the previous [19] and the newly proposed methods. The measurement position was the center of the femur and the diaphysis specimen respectively (Fig. 1). The bone marrow and the soft tissue around the surfaces were removed and the specimen was air dried at room temperature.

2.2 Measurements using XRD-IP system

This study evaluates the cortical bone in the diaphysis of extremities as an orthotropic compound. Additionally, the residual stress state in the measurement region was assumed to be a plane stress because the used X-rays could only penetrate

approximately 100 μm of the specimens, measuring only the outermost region.

Figure 2(a) shows the measurement setup of the XRD-IP system. The diaphysis specimen was irradiated with characteristic X-rays and the resulting diffracted X-rays were detected by the IP in the reflection side. As shown in Fig. 2(a), the *x*-*y*-*z* coordinate system is fixed at the specimen surface and the *x*-, *y*-, and *z*-axes correspond to the bone axial, circumferential, and radial directions, respectively. The *x*'-*y*'-*z*' coordinate system is defined as the X-ray coordinate system and the incident X-rays enter the specimen along the *y*'-axis. The *x*'-axis corresponds to the *x*-axis and the angle between the *y*'- and *y*-axes is set to 7.25°, which is the Bragg angle θ_0 of the (211) lattice planes in the HAp crystals in a non-strained state using the characteristic Mo-Kα X-rays from the ICDD-PDF (International Center for Diffraction Data - Powder Diffraction Files) No. 9-432. The *X*'-*Y*'-*Z*' coordinate system is fixed at the IP surface and the *Y*'-axis corresponds to the *y*'-axis. The *1*-, *2*-, and *3*-axes are the principal axes and the *3*-axis corresponds to the *z*-axis as shown in Fig. 2(b). The angle φ is defined as the angle between the *1*- and *x*-axes.

Bone tissue deformation affects the interplanar spacing *d* of the HAp crystals

in the tissue. The angle of inclination ψ is defined as the angle between the normal direction of the specimen surface and the diffracted lattice plane. As shown in Fig. 2(c), under tensile residual stress σ_x, the interplanar spacing of the lattice planes at $\psi = 90°$ is larger than that at $\psi = 0°$. The relationship between d and ψ is affected by the magnitude of the stress.

The HAp crystal strain ε^H is defined in equation (1), where d_0 is the interplanar spacing of the non-strained state.

$$\varepsilon^H = \frac{d - d_0}{d_0} \tag{1}$$

This study presumed the relationship between the bone tissue stress σ^B and the HAp crystal strain ε^H in the cortical bone as described in equation (2).

$$\begin{pmatrix} \varepsilon_x^H \\ \varepsilon_y^H \\ \varepsilon_z^H \end{pmatrix} = \begin{bmatrix} \frac{1}{E^*} & -\frac{\nu^*}{E^*} & -\frac{\nu^*}{E^*} \\ -\frac{\nu^*}{E^*} & \frac{1}{E^*} & -\frac{\nu^*}{E^*} \\ -\frac{\nu^*}{E^*} & -\frac{\nu^*}{E^*} & \frac{1}{E^*} \end{bmatrix} \begin{pmatrix} \sigma_x^B \\ \sigma_y^B \\ \sigma_z^B \end{pmatrix} \tag{2}$$

The XRD pattern, which is a portion of the Debye ring of (211) lattice planes in HAp crystals, was detected by the IP. The traveling direction of the diffracted X-rays depends on the direction and the displacement of the lattice planes in the HAp crystals. In the β-direction on the IP, the radius r_β of the Debye ring reflects the diffraction angle $2\theta_\beta$ and the sample-detector distance L as shown in Fig. 2(a) and expressed by equation (3).

$$r_\beta = L \tan 2\theta_\beta \tag{3}$$

Then, the HAp crystal strain in the direction corresponding to the β-direction on IP, ε^H_β, is described with $2\theta_\beta$ as shown in equation (4).

$$\varepsilon^H_\beta = \frac{d_\beta - d_0}{d_0} = \frac{\sin\theta_0 - \sin\theta_\beta}{\sin\theta_\beta} \tag{4}$$

Here, the direction of ε^H_β is slightly inclined at an angle of $\Delta\varphi$ from the x-z plane toward

the *y*-axis with increasing β, as shown in Fig. 2(b). The angles $\Delta\varphi$ and ψ as shown in Fig. 2(b) are related to β by equations (5) and (6), respectively.

$$\Delta\phi = \tan^{-1}\left\{\frac{\cos\theta_0(\tan\theta_\beta - \tan\theta_0\cos\beta)}{\sin\beta}\right\} \quad (5)$$

$$\psi = \cos^{-1}(\cos\theta_0\cos\theta_\beta\cos\beta + \sin\theta_0\sin\theta_\beta) \quad (6)$$

$\varepsilon^H{}_\beta$ is described with respect to $\varepsilon^H{}_1$, $\varepsilon^H{}_2$, and $\varepsilon^H{}_z$ as in equation (7).

$$\varepsilon_\beta^H = \{\varepsilon_1^H\cos^2(\phi+\Delta\phi) + \varepsilon_2^H\sin^2(\phi+\Delta\phi)\}\sin^2\psi + \varepsilon_z^H(1-\sin^2\psi) \quad (7)$$

$\varepsilon^H{}_x$ is also described with respect to $\varepsilon^H{}_1$ and $\varepsilon^H{}_2$ as in equation (8).

$$\varepsilon_x^H = \varepsilon_1^H\cos^2\phi + \varepsilon_2^H\sin^2\phi \quad (8)$$

Here $\Delta\varphi$ is presumed as negligibly small, because the Debye ring is only detected in the range between β = -40° and β = 40° in this study and the effects of θ_β changes due to the

stress is very small in equation (5). Hence, $\cos^2(\varphi+\Delta\varphi)$ and $\sin^2(\varphi+\Delta\varphi)$ are approximated as $\cos^2\varphi$ and $\sin^2\varphi$, respectively. Then, ε^H_β is described as equation (9) using this approximation.

$$\varepsilon_\beta^H = \varepsilon_x^H \sin^2\psi + \varepsilon_z^H (1-\sin^2\psi) \tag{9}$$

Therefore, ε^H_β is described by equation (10) using equation (2).

$$\varepsilon_\beta^H = \frac{1+\nu^*}{E^*}\sigma_x^B \sin^2\psi - \frac{\nu^*}{E^*}(\sigma_x^B + \sigma_y^B) \tag{10}$$

From the partial differentiation of equation (10) with respect to $\sin^2\psi$, the following expression is derived.

$$\sigma_x^B = \frac{E^*}{1+\nu^*}\frac{\partial \varepsilon_\beta^H}{\partial(\sin^2\psi)} \tag{11}$$

Using Bragg's law, σ^B_x can be described with ψ and $2\theta_\beta$ in degrees as in equation (12),

where K_x is a stress constant and the K_x value was measured using a four-point bending test of a bone specimen with X-ray irradiation in the previous study [19].

$$\sigma_x^B = \left\{ -\frac{E^*}{2(1+\nu^*)}\frac{\pi}{180}\cot\theta_0 \right\}\frac{\partial(2\theta_\beta)}{\partial(\sin^2\psi)} \equiv K_x \frac{\partial(2\theta_\beta)}{\partial(\sin^2\psi)} \tag{12}$$

Therefore, the macroscopic residual stress in the bone axial direction can be calculated via the portion of the Debye ring of (211) lattice plane in HAp crystals detected by the IP in the reflection side. The calculated stress is the deviatoric stress because the hydrostatic deformation resulting from hydrostatic stress cannot be detected.

2.3 Measurement conditions

The measurements on the specimen surface were conducted five times at four positions: anterior, posterior, lateral, and medial (Fig. 1). An X-ray diffractometer (RINT2200: Rigaku, Japan) was used to generate characteristic Mo-Kα X-rays (λ = 0.071 nm). The incident X-rays were collimated using a collimator with a diameter of

1.0 mm and the Kβ X-rays were eliminated using a thin Zr filter. The XRD pattern was detected with an IP (1150×1150 pixel^2) (BAS-SR 127×127 mm^2, FUJIFILM, Japan) and the sample-detector distance L was 180 mm.

Since an accurate position of the beam center on the XRD pattern is required to measure r_β for equation (12) in this method, X-ray irradiation was carried out twice for one stress measurement. First, the XRD measurement was carried out and the XRD pattern was detected via an IP that was partially covered with a thick copper plate to exclude the direct beam of incident X-rays. Second, after the specimen and the copper plate were removed from the setup, the X-rays penetrated the same IP above the previous pattern to obtain the position of the beam center as the origin of the Debye ring. Then, the IP was scanned (R-axis DS3C, Rigaku, Japan) to obtain the distribution of X-ray intensity.

For the first irradiation, the left part of the IP was covered by a copper plate with a thickness of 3 mm, as shown in Fig. 2(a). The diaphysis specimen was irradiated with X-rays for 300 s; the tube voltage was 40 kV, and the tube current was 40 mA. For the second irradiation, the X-rays penetrated the IP for 1 s with a tube voltage of 20 kV

and a tube current of 2 mA.

The Debye ring in the XRD pattern included the diffraction of not only the (211) lattice plane but also (112) and (300) lattice planes of the HAp crystals. The study defined r_β as the radius of the synthetic Debye ring, as did the previous studies [19, 20]. The diffraction profiles, which are the relationships between the intensity of the diffracted X-rays, I, and the radius r, were obtained with a resolution of the r of 1 pixel from the XRD pattern at intervals of 1° from β = 0° to 40°. The r_β was determined to be the midpoint of the full width at two-thirds maximum intensity (FWTTM) of each profile. The residual stress σ^B_x was calculated using equation (12) from the distribution of r_β obtained from the 41 profiles via the linear least-squares method.

2.4 Measurements using previous method

To evaluate the expediency of the proposed method, the residual stresses in the same specimen were measured using the previous method [19]. The XRD measurements were conducted with respect to ψ: from ψ = 0° to 40° at 10° intervals. The specimen was irradiated with the collimated X-rays at a tube voltage of 40 kV, a

tube current of 40 mA, and an exposure time of 180 s. A diffraction profile was obtained from 2θ = 13.0° to 16.0° by scanning a scintillation counter. The total exposure time was 900 s for one stress measurement.

3. Results

Figure 3 shows the typical XRD pattern of the anterior position detected by the IP. In the right part of the image, the Debye ring from the HAp crystals was observed. In the left part, the XRD pattern was not observed because the IP was covered with a thick copper plate for the first irradiation. For the second irradiation, only the beam center was clearly observed. As shown in Fig. 3, the r-β polar coordinate system was fixed at the beam center and the diffraction profiles were obtained for each β. Figure 4 shows the diffraction profiles at β = 0° and 40° in the XRD pattern shown in Fig. 3. The lines indicate smoothed profiles obtained using the simple moving average method. In this case, the peak position in the profile at β = 40° shifted to the left as compared to the peak position at β = 0°.

Figure 5 shows the relationships between 2θ calculated from r_β with equation (3) and $\sin^2\psi$ calculated from β with equation (6) in five measurements at the anterior (Fig. 5(a)) and posterior (Fig. 5(b)) positions. The circular and triangular marks indicate the values from the XRD-IP system and the previous method respectively and the same color indicates the values from an identical measurement. The average gradients of the relationship $\partial(2\theta)/\partial(\sin^2\psi)$ at the anterior and posterior positions measured by the XRD-IP system were -0.22 ± 0.01° and -0.05 ± 0.01°, respectively. The average R^2 value at the anterior position was 0.69 ± 0.06 and there was a strong linearity between 2θ and $\sin^2\psi$. In the previous method, the average gradients at the anterior and posterior positions were -0.18 ± 0.01° and -0.03 ± 0.02°, respectively. The average standard deviations of the gradient at the four positions using the XRD-IP system and the previous method were 0.02° and 0.01°, respectively. Further, the average standard deviations of 2θ in five measurements at the four positions using the XRD-IP system and the previous method were 0.02° and 0.01°, respectively.

Figure 6 shows the residual stress distribution at the diaphyseal surface of the bovine femur measured by both the XRD-IP system and the previous method. The

anterior (146 MPa), lateral (135 MPa), and medial (117 MPa) positions were subjected to higher tensile stresses than the posterior position (34 MPa) according to the measurements using the XRD-IP system. The trend corresponds to the previous report on bovine femurs [19, 21, 22]. The average difference of the values of calculated residual stresses between the two methods for all four positions was 18 MPa. Although the standard deviation of residual stress in the XRD system was slightly larger than that in the previous methods, the values of residual stresses were almost the same as the results of the previous method.

4. Discussions

This study developed a measurement system with an IP for obtaining the surface distribution of residual stress in the diaphysis of extremities and obtained tensile residual stresses at the surface of the bovine femoral diaphysis, corresponding to the results of the previous method. This system detected only the deviatoric stress and this study focused on the distribution of that stress. The system reduced the irradiation time

by two thirds and derestricted the sample size in the longitudinal direction. This system can be used to obtain measurements of the surface stress distribution of the diaphysis in whole bones in vitro and in situ. Furthermore, the system can be also applied to external stress measurements by comparing stress distributions before and after loading.

The stress states of cortical bone and trabecular bone in the inner region of the diaphysis cannot be measured using the current system. The structure and the mechanical properties of trabecular bone may sensitively change with bone diseases. It is also interesting to focus on the changes of the surface stress state along the changes in the inner region.

According to Fig. 3, the Debye ring and the beam center can be obtained using the simple setup including an X-ray generator, a collimator, and an IP in a short irradiation time to calculate the residual stress. The radius of the Debye ring was accurately obtained using the two-step irradiation. When the Debye ring and the beam center are obtained using only one irradiation, the direct beam is partially absorbed by the sample and the measured position of the beam center shifts. Hence, the shift changes the distribution of r_β and the value of residual stress. The two-step irradiation process is

important for measuring the diffracted X-rays from the bone surface in the reflection side.

Further, as suggested in Fig. 5, the resolution of $\sin^2\psi$ can be increased using the IP, depending on the readout resolution of the scanner. High resolution is important for confirming the linearity of the relationship between 2θ and $\sin^2\psi$ and therefore calculating the residual stress. The study assumed that the residual stress state in the measurement region was under plane stress. If this assumption is not satisfied, the relationship does not have linearity. In this study, it was confirmed that the relationship had enough linearity as being shown in Fig. 5.

However, the standard deviation of 2θ was larger than that of the previous method. This may be related to the limitations of the current system: a slight variation in the L among the five measurements. In the previous method, the variation of L negligibly affected 2θ because of a parallel X-ray beam obtained using a soller slit, a scintillation counter, and a goniometer. In the current system, the variation affected the standard deviation of 2θ and $\partial(2\theta)/\partial(\sin^2\psi)$, although it may hardly affect the values of residual stress. The standard deviation of $\partial(2\theta)/\partial(\sin^2\psi)$ in the only five profiles at the

same ψ conditions of the previous method was quite larger than that from all profiles. Further, the value of $\partial(2\theta)/\partial(\sin^2\psi)$ decreased to 64% at the medial position resulting from the decrease of R^2. In this case, the high resolution of $\sin^2\psi$ suppressed the standard deviations of $\partial(2\theta)/\partial(\sin^2\psi)$ and residual stress. To increase the sensitivity of the detector will contribute further accuracy improvement.

As shown in Fig. 6, the tensile residual stresses along the bone axis were obtained at the diaphyseal surface. This corresponds to our previous reports [19-22]. Other studies using high-energy X-rays and a two-dimensional detector investigated the compressive residual stress/strain in the mineral phase along the bone axis using a rat tibia [9] and canine fibulas [3, 7]. However, the stress/strain was the weighted average of the X-ray pathway from the irradiated surface to the opposite surface of the diaphysis. Although it is difficult to compare the current result and this directly, the difference may be explained by the compressive residual stress in the deeper region of adult bovine femurs [22].

The detailed deformation behavior of HAp crystals inside the tissues can be obtained by the method using high-energy X-rays and a two-dimensional detector [3, 5,

7, 9-12, 14, 15]. Further, the method can also be applied to the collagen phase [3, 5, 7, 10]. However, Singhal et al. reported that the residual strain in the mineral phase markedly changed with increasing high-energy X-ray doses because of the damage at the HAp-collagen interface in bone tissue [26]. To study the bone residual stresses, it is important to minimize the X-ray energy and irradiation time such as the current system.

This study presumed the relationship between σ^B and ε^H in cortical bone as isotropic and calculated residual stresses from the relationship between d and ψ. The relationships may be locally affected by the nonuniform structures of the tissue that is derived from the osteon formation and the internal organization down to the nanostructural level and results in the variation of elastic modulus of cortical bone [13, 27-28]. However, the stress constant was not significantly different in both the bone axial and circumferential directions [19] and could be considered as the same value independently of the distribution of elastic modulus in the XRD measured regions as discussed in [20]. Hence, it appears that the assumption is reasonable and may have less impact on the results in this method.

Further, to obtain equation (9), $\cos^2(\varphi+\Delta\varphi)$ and $\sin^2(\varphi+\Delta\varphi)$ were

approximated as $\cos^2\varphi$ and $\sin^2\varphi$ respectively in this method. The maximum $\Delta\varphi$ at β = 40° was 2.71° and the error of the assumption was smaller than 0.05 in this study. It appears that the assumption may have less impact on the calculation of residual stresses.

A limitation of this result was the use of the air-dried specimen cut out from a whole bone due to comparison with the previous method. The cutting process in this study may have less impact on the measured residual stresses, according to the result of the strain gauge measurement during the same cutting process [22]. Further, the effects of air-drying process might also have less impact on the measured deviatoric stresses, although there may be hydrostatic compressive deformation related with the sample volume changes due to the air-drying. A further study of these effects should be conducted.

There are still some limitations for applying this system to in vivo stress measurements. To obtain the diffracted X-rays passing through the periosteum, muscles, and subcutaneous fat layer above the skin, it is necessary to detect only the diffracted X-rays from the HAp crystals with a sufficient sensitivity. Fujisaki et al. and Tadano et al. proposed a novel method for quantifying the HAp crystal strain from the diffusive

XRD profiles [4, 8]. Furthermore, Fujisaki and Tadano reported the conditions for measuring the strain of pure titanium covered with soft tissue using XRD and the availability of characteristic Mo-Kα X-rays, which facilitates the in vivo evaluation of the stress and crystal conditions of materials [29]. This knowledge will further improve the XRD-IP system for noninvasive in vivo measurements of bone stress.

Acknowledgements

This work was supported by a Grant-in-Aid for Scientific Research (A), MEXT (No. 24240068).

References

[1] Al Nazer R, Lanovaz J, Kawalilak C, Johnston JD, Kontulainen S (2012) Direct in vivo strain measurements in human bone - A systematic literature review. J Biomech 45:27-40

[2] Tadano S, Giri B (2011) X-ray diffraction as a promising tool to characterize bone nanocomposites. Sci Technol Adv Mater 12:064708

[3] Almer JD, Stock SR (2005) Internal strains and stresses measured in cortical bone via high-energy X-ray diffraction. J Struct Biol 152:14-27

[4] Fujisaki K, Tadano S, Sasaki N (2006) A method on strain measurement of HAP in cortical bone from diffusive profile of X-ray diffraction. J Biomech 39:579-586

[5] Gupta HS, Seto J, Wagermaier W, Zaslansky P, Boesecke P, Fratzl P (2006) Cooperative deformation of mineral and collagen in bone at the nanoscale. Proc Natl Acad Sci USA 103:17741-17746

[6] Fujisaki K, Tadano S (2007) Relationship between bone tissue strain and lattice strain of HAp crystals in bovine cortical bone under tensile loading. J Biomech

40:1832-1838

[7] Almer JD, Stock SR (2007) Micromechanical response of mineral and collagen phases in bone. J Struct Biol 157:365-370

[8] Tadano S, Giri B, Sato T, Fujisaki K, Todoh M (2008) Estimating nanoscale deformation in bone by X-ray diffraction imaging method. J Biomech 41:945-952

[9] Stock SR, Yuan F, Brinson LC, Almer JD (2011) Internal strain gradients quantified in bone under load using high-energy X-ray scattering. J Biomech 44:291-296

[10] Dong XN, Almer JD, Wang X (2011) Post-yield nanomechanics of human cortical bone in compression using synchrotron X-ray scattering techniques. J Biomech 44:676-682

[11] Akhtar R, Daymond MR, Almer JD, Mummery PM (2011) Lattice strains and load

partitioning in bovine trabecular bone. Acta Biomater 7:716-723

[12] Giri B, Almer JD, Dong XN, Wang X (2012) In situ mechanical behavior of mineral crystals in human cortical bone under compressive load using synchrotron X-ray scattering techniques. J Mech Behav Biomed Mater 14:101-112

[13] Yamada S, Tadano S, Fujisaki K, Kodaki Y (2013) Influence of osteon area fraction and degree of orientation of HAp crystals on mechanical properties in bovine femur. J Biomech 46:31-35

[14] Deymier-Black AC, Almer JD, Stock SR, Haeffner DR, Dunand DC (2010) Synchrotron X-ray diffraction study of load partitioning during elastic deformation of bovine dentin. Acta Biomater 6:2172-2180

[15] Almer JD, Stock SR (2010) High energy X-ray scattering quantification of in situ-loading-related strain gradients spanning the dentinoenamel junction (DEJ) in

bovine tooth specimens. J Biomech 43:2294-2300

[16] Fujisaki K, Todoh M, Niida A, Shibuya R, Kitami S, Tadano S (2012) Orientation and deformation of mineral crystals in tooth surfaces. J Mech Behav Biomed Mater 10:176-182

[17] Tadano S, Okoshi T (2006) Residual stress in bone structure and tissue of rabbit's tibiofibula. Biomed Mater Eng 16:11-21

[18] Giri B, Tadano S, Fujisaki K, Todoh M (2008) Understanding site-specific residual strain and architecture in bovine cortical bone. J Biomech 41:3107-3115

[19] Yamada S, Tadano S (2010) Residual stress around the cortical surface in bovine femoral diaphysis. J Biomech Eng 132:044503

[20] Yamada S, Tadano S, Fujisaki K (2011) Residual stress distribution in rabbit limb

bones. J Biomech 44:1285-1290

[21] Yamada S, Tadano S, Todoh M, Fujisaki K (2011) Residual stress distribution in the bovine femoral diaphysis measured by synchrotron. J Biomech Sci Eng 6:114-124

[22] Yamada S, Tadano S (2013) Effects of growth on residual stress distribution along the radial depth of cortical cylinders from bovine femurs. J Biomech 46: 2130-2136

[23] Fung YC (1990) Biomechanics: Motion, Flow, Stress, and Growth. Springer, USA

[24] Mason MW, Skedros JG, Bloebaum RD (1995) Evidence of strain-mode-related cortical adaptation in the diaphysis of the horse radius. Bone 17:229-237

[25] Skedros JG, Mendenhall SD, Kiser CJ, Winet H (2009) Interpreting cortical bone adaptation and load history by quantifying osteon morphotypes in circularly polarized light images. Bone 44:392-403

[26] Singhal A, Deymier-Black AC, Almer JD, Dunand DC (2011) Effect of high-energy X-ray doses on bone elastic properties and residual strains. J Mech Behav Biomed Mater 4:1774-1786

[27] Rho JY, Zioupos P, Currey JD, Pharr GM (2002) Microstructural elasticity and regional heterogeneity in human femoral bone of various ages examined by nano-indentation. J Biomech 35:189–198

[28] Gibson VA, Stover SM, Gibeling JC, Hazelwood SJ, Martin RB (2006) Osteonal effects on elastic modulus and fatigue life in equine bone. J Biomech 39:217–225

[29] Fujisaki K, Tadano S (2010) Strain measurement of pure titanium covered with soft tissue using X-ray diffraction. J Biomech Eng 132:031004

Legends

Fig. 1 Measurement positions at the diaphyseal surface of a bovine femur

Fig. 2 (a) Measurement setup of the XRD-IP system. The *x*-*y*-*z* coordinate system is fixed at the specimen surface and the *x*-, *y*-, and *z*-axes correspond to the bone axial, circumferential, and radial directions, respectively. The *x*'-*y*'-*z*' coordinate system is defined as the X-ray coordinate system and the incident X-rays enter the specimen along the *y*'-axis. The *x*'-axis corresponds to the *x*-axis and the angle between the *y*'- and *y*-axes is set at θ_0. The *X*'-*Y*'-*Z*' coordinate system is fixed at the IP surface and the *Y*'-axis corresponds to the *y*'-axis. Incident X-rays enter the specimen along the *y*'- and *Y*'-axes. The arrow ε^{H}_{β} indicates the normal direction of the diffracted lattice plane of HAp crystals contributing to the XRD to the β-direction on IP. (b) The relationship among *x*-*y*-*z*, *x*'-*y*'-*z*', and *1*-*2*-*3* coordinate systems and the direction of ε^{H}_{β}. The *1*-, *2*-, and *3*-axes are the principal axes and the *3*-axis corresponds to the *z*-axis. The angle φ is defined as the angle between the *1*- and *x*-axes. The residual stress state in the

measurement region was presumed to be a plane stress. The angle ψ is defined as the angle between the *z*-axis and the direction of ε^{H}_{β}. (c) Schematic of the variation of the interplanar spacing of HAp crystals under tensile residual stress σ_x in the measurement position. The interplanar spacing of lattice planes in the ψ = 90° direction is larger than that in the ψ = 0° direction ($d_1 < d_2 < d_3$). The relationship is dependent on the magnitude of the stress

Fig. 3 Typical XRD pattern of the anterior position detected by IP. In the right part of the image, the Debye ring from the HAp crystals is observed. In the left part, since the IP is covered with a thick copper plate for the first irradiation, the XRD pattern is not observed and only the beam center is clearly observed from the second irradiation

Fig. 4 Diffraction profiles at β = 0° and 40° in the XRD pattern as shown in Fig. 3

Fig. 5 Relationships between 2θ and $\sin^2\psi$ in five measurements at (a) the anterior and (b) the posterior positions. The circular and triangular marks indicate the values from

the XRD-IP system and the previous method respectively and the same color indicates the values from an identical measurement. The normal and dash lines indicate regression lines of the data from XRD-IP system and the previous method, respectively

Fig. 6 Residual stress distribution at the diaphyseal surface of the bovine femur measured by the XRD-IP system and the previous method

Figures

Figure 1

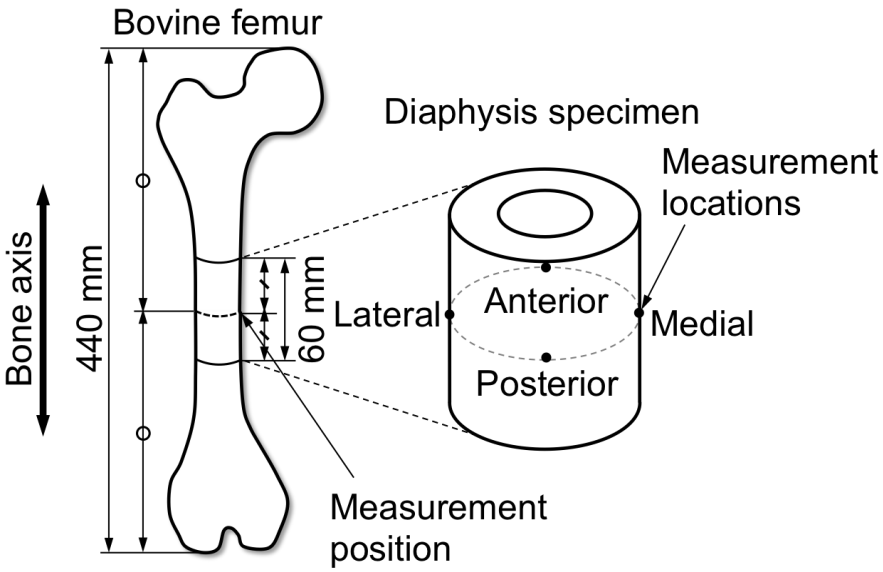

Figure 2

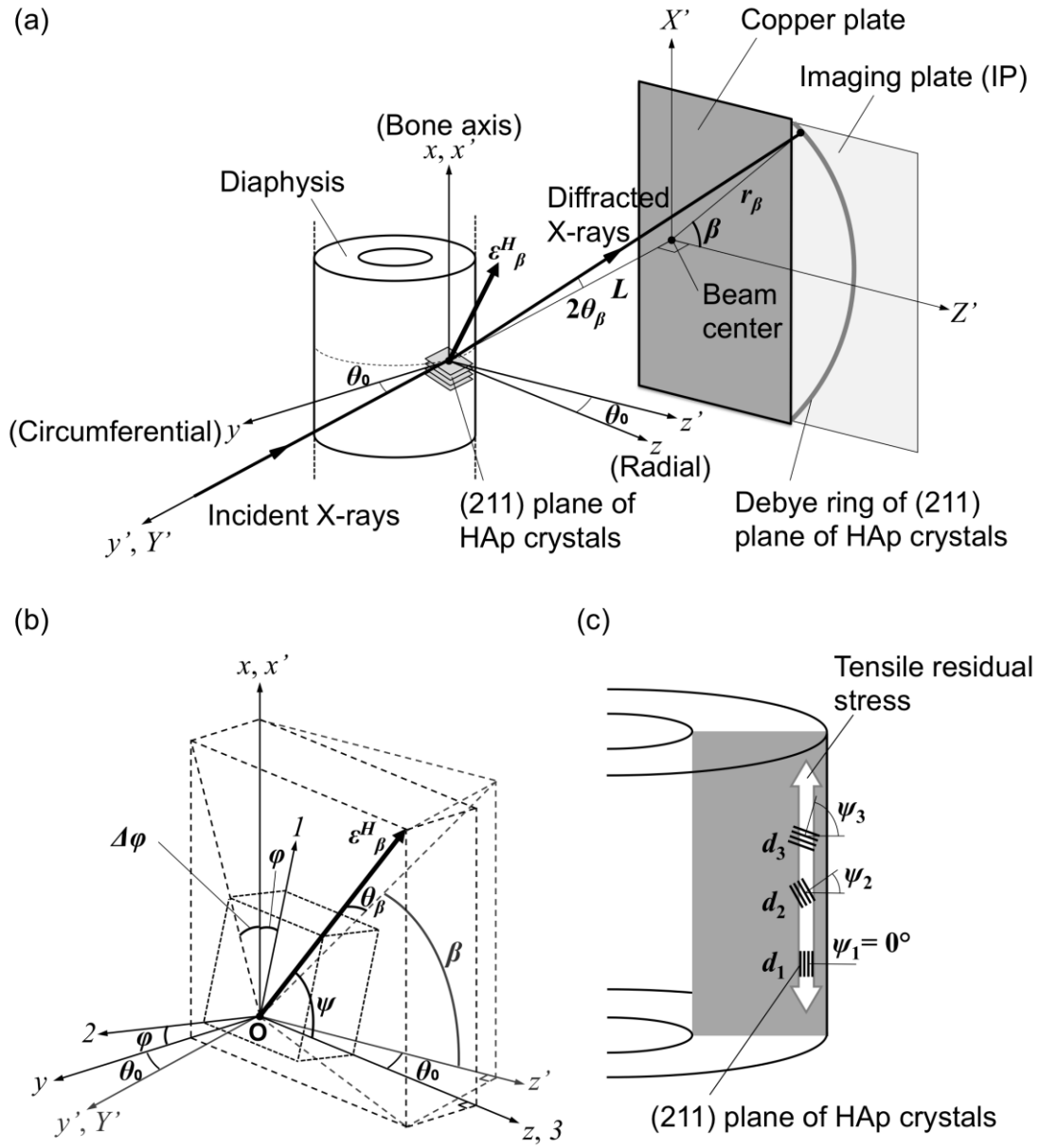
(a)
X'
Copper plate
Imaging plate (IP)
(Bone axis)
x, x'
Diaphysis
Diffracted
X-rays
r_β
β
$\varepsilon^H{}_\beta$
L
$2\theta_\beta$
Beam
center
Z'
θ_0
(Circumferential) y
θ_0
z'
z
(Radial)
Incident X-rays
y', Y'
(211) plane of
HAp crystals
Debye ring of (211)
plane of HAp crystals
(b)
x, x'
$\Delta\varphi$
1
φ
$\varepsilon^H{}_\beta$
θ_β
β
ψ
2
φ
O
y
θ_0
θ_0
z'
y', Y'
z, 3
(c)
Tensile residual
stress
ψ_3
d_3
ψ_2
d_2
$\psi_1 = 0°$
d_1
(211) plane of HAp crystals

Figure 3

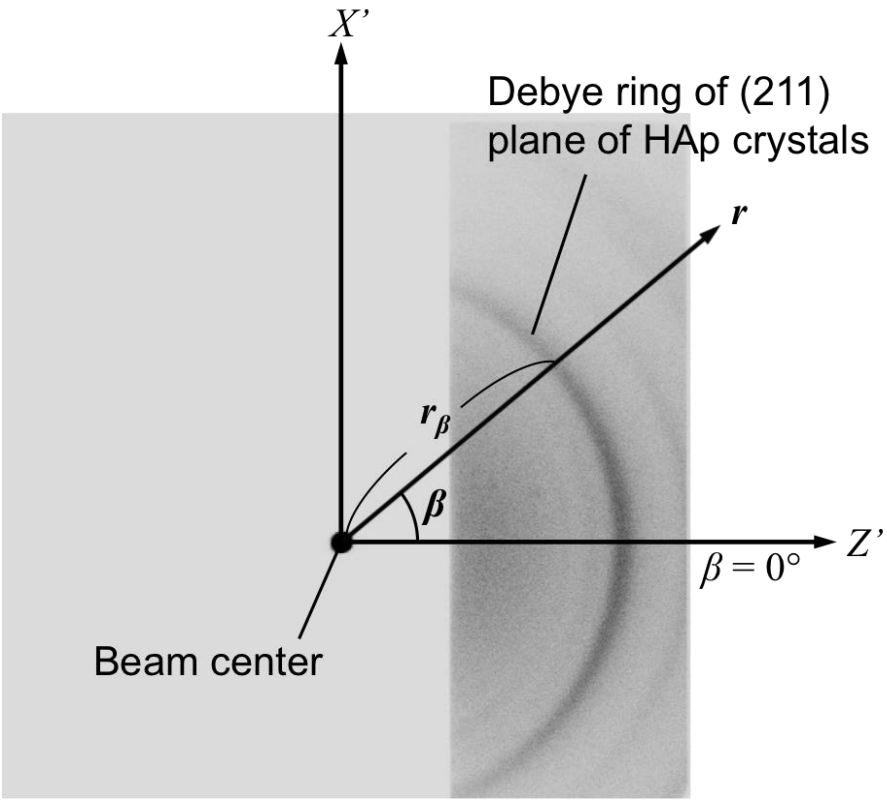
X'
Debye ring of (211)
plane of HAp crystals
r
r_β
β
Z'
$\beta = 0°$
Beam center

Figure 4

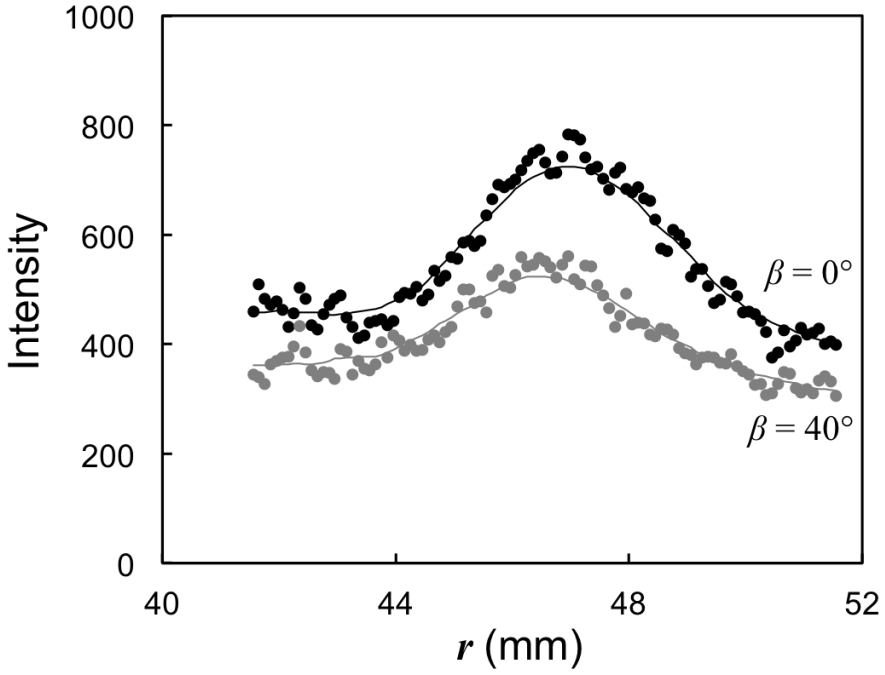

Figure 5

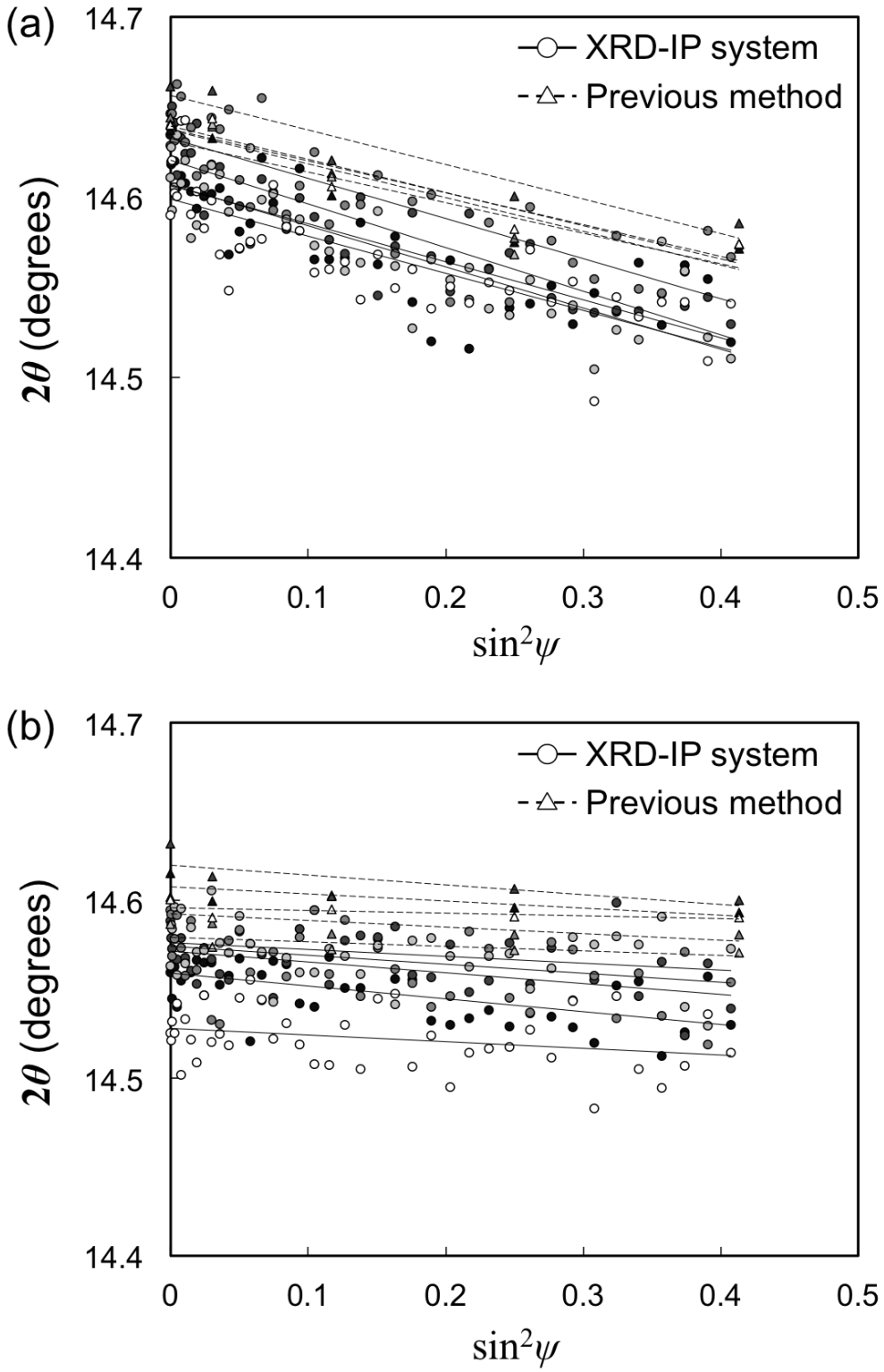
(a)
XRD-IP system
Previous method
2θ (degrees)
14.7
14.6
14.5
14.4
0
0.1
0.2
0.3
0.4
0.5
sin²ψ
(b)
XRD-IP system
Previous method
2θ (degrees)
14.7
14.6
14.5
14.4
0
0.1
0.2
0.3
0.4
0.5
sin²ψ

Figure 6

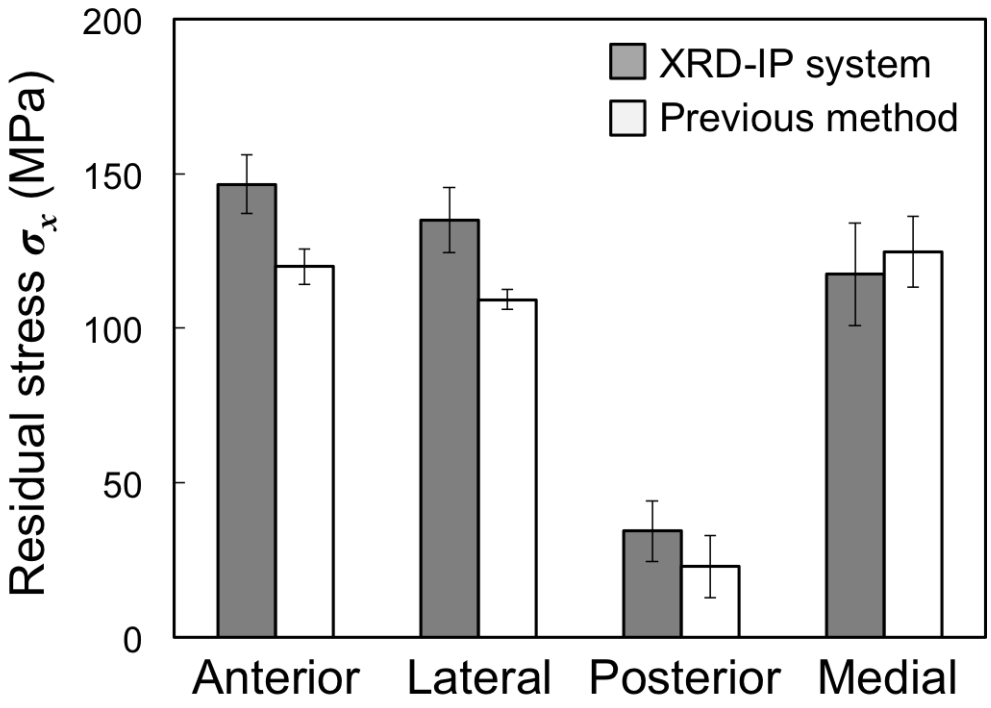
200
150
100
50
0
Residual stress σ_x (MPa)
XRD-IP system
Previous method
Anterior
Lateral
Posterior
Medial